The Horizontal Eddies in the Offshore Zone

Li Li[1], Robert A. Dalrymple[2]

Abstract:

The mean flow outside the surf zone can be unstable and form a train of submerged vortices, which migrate slowly in the offshore direction, as discovered by Matsunaga , Takehara & Awaya (1988, 1994). Li and Dalrymple (1998) conducted large scale experiments and a numerical study. They showed that two layers of vortices could exist over the water depth. Eddies near the water surface rotated in the opposite direction of eddies at mid-depth. For example, for the surface wave propagating to the right, the rotation direction of eddies near mid-depth was counterclockwise, while the rotation direction of eddies near surface was clockwise. The vortices decay offshore where there was no shear layers over water depth. Experimental and numerical studies show the velocity of long time scale vortical motion is uniform over water depth and is much slower than the undertow. A theoretical analysis showes that the stresses due to turbulence and wave serve as the source of the vorticity and this vortex train is formed by the shear instabilities of the mean flow in the cross-shore direction.

1   Introduction

The nearshore circulation system induced by wave breaking plays an important role in sediment transport. This circulation system (longshore, rip and cross-shore currents) has been studied for years to develop predictive models. The theory of longshore currents changed abruptly with the introduction of radiation stresses, which codified the momentum input to the surf zone by the waves; and lateral mixing, which is

---

[1]Graduate Student, Center for Applied Coastal Research, Department of Civil and Environment Engineering, University of Delaware, Newark, DE 19716, USA.

[2]Professor, Department of Civil and Environment Engineering, Center for Applied Coastal Research, University of Delaware, Newark, DE 19716, USA

necessary to create a smooth transition of longshore current from onshore to offshore of the breaker line.

In addition to the longshore currents, there are cross-shore currents flowing perpendicularly to the shoreline. The cross-shore currents consist of the mass transport to the shoreline carried by waves and return flow known as undertow. The undertow inside the surf zone has drawn much attention in the literature (e.g. Nadaoka et al. (1982), Svendsen et al. (1992), Okayasu et al. (1992) and Cox et al. (1995)).

Matsunaga et al. (1988, 1994) conducted a experiment on the flow outside the surf zone in a small wave tank (12 m long, 0.4 m deep, 0.15 m wide and equipped with a sloping planar bed). They discovered that the mean flow in the cross-shore direction outside the surf zone could be unstable and formed a single layer vortex train. The vortices rotate at the direction opposite the direction of the wave-induced water particle trajectories. They also found that these offshore migrating vortices would decay when it reached the region with deeper water depth. The formation of eddies is independent of the breaker type. Li and Dalrymple (1998) studied this offshore vortex train and concluded that the vortices formed due to the instability of undertow seaward of the breaker line. They also found that the vortices decayed when the velocity profile of the undertow becomes linear over the water depth.

Bagnold (1947) studied mass transport outside the surf zone by experiments. He discovered that there were a fast shoreward current along the bed and a slow seaward current under the water surface when two-dimensional surface wave propagating over a horizontal smooth bed. This phenomenon is due to the existence of Stokes layer and viscosity (Longuet-Higgins (1953)). Dore (1970) studied the mass transport outside the surf zone theoretically by taking into account the air-water interface. He concluded that on a clean interface the surface viscosity greatly affected the drift velocity of short waves and the air boundary layer greatly affected the long waves. The mean Eulerian velocity near the surface which is in the onshore direction had a greater onshore velocity than the Stokes drift. On the study of clean and contaminated fluid, Craik (1982) obtained similar results. Through a experimental study, Nadaoka et al. (1982) obtained linear velocity profile outside of the breaker line: a weak seaward velocity at the bed and a strong seaward velocity under the trough level. Cox et al. (1995) obtained similar velocity profile on the experiment of regular waves spilling on a 1 : 35 impermeable slope. Okayasu et al. (1992) conducted detailed laboratory measurements of the undertow due to regular and random waves on a 1 : 20 smooth uniform slope. Rather than a straight-line distribution over the depth outside the surf zone, their measured undertow velocity profiles are curved; it has a shoreward directed velocity at the bed and a seaward oriented velocity under the trough level. In the present study, we obtained the velocity profiles experimetally at the place where the vortices can be observed and at the place that the vortices decayed. This paper also investigate the offshore vortices experimentally and numerically.

2   Experimental Set-up

The wave experiments were conducted in a Precision Wave Tank (PWT) at the Center of Applied Coastal Research at the University of Delaware. This section describes the experimental setup and data acquisition procedure.

The experimental wave tank was 35 m long, 0.6 m deep and 0.6 m wide. It was 3 times longer, 4 times wider and 1.5 times deeper than the wave tank used by Matsunaga *et al.* (1988, 1994). Figure 1 shows a schematic of the experimental setup. The region at the wavemaker had constant depth, and the region at the other end had a sloping planar bed with 1 : 35 slope. A piston wavemaker was used to generate the two-dimensional periodic surface waves. As shown in Figure 1, three 3-D Acoustic Doppler Velocimetries (ADV) were used to obtain the Eulerian velocity outside of the surf zone. Two capacitance wave gages were used to measure the local wave height H and wave period T. The local phase velocity C was calculated from the time lag of signals from two wave gages that were located 20 cm apart. The local wavelength L was then determined from the product of the celerity and wave period.

The vortex train offshore of the breaker point was observed by flow visualization. Granules of water-soluble aniline blue dye was used as a tracer. Flow patterns were photographed through the glass sidewall of the tank using a 35 mm camera.
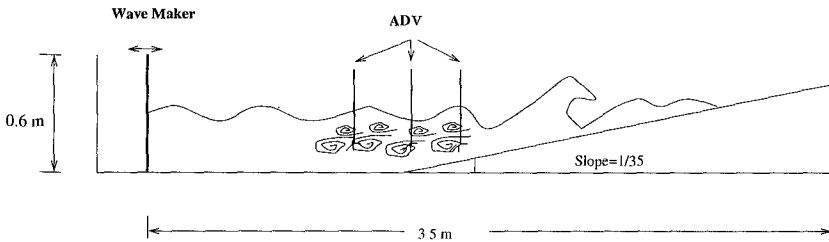

Figure 1: Schematic of experiment set-up.

Based on Matsunaga et al. (1994) (Figure 2), eight tests were designed to explore the effects of varying local water depth h and wave frequencies on the offshore vortex train (Table 1). Tests 1 through 4 were designed in the formation region: the combinations of the dimensionless wave height (H/L) and dimensionless water depth (h/L) would always generate vortices. Test 5 and Test 6 were in the region where the occurrence of vortex varies. Test 7 and Test 8 were designed in the region that no vortices were observed.

Table 1: List of Experiments

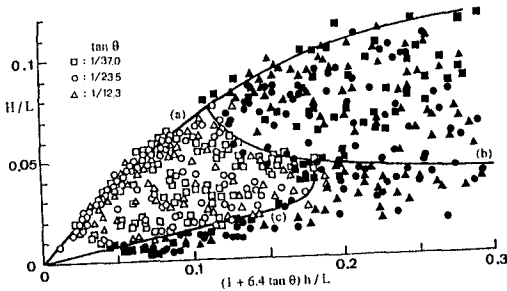| Test	Wave Period (s)	Water Depth (m)	h/L	H/L	Existence of Vortices
1	2.0	0.303	0.0925	0.0272	yes
2	2.0	0.310	0.0946	0.0267	yes
3	2.0	0.275	0.0878	0.0301	yes
4	2.0	0.313	0.0942	0.0285	yes
5	1.4	0.270	0.1306	0.0676	yes
6	1.4	0.381	0.1619	0.0594	yes
7	1.1	0.310	0.2057	0.0970	no
8	1.1	0.418	0.2580	0.0900	no

Figure 2: Formation regions of offshore vortices from Matsunaga, Takehara & Awaya (1994): open symbols, formation of offshore vortex; solid symbols, non-formation. Lines (a) and (b) indicate the limit of wave steepness and $H_0/L_0 = 4.2 \times 10^{-2}$, respectively. Line (c) is the offshore border of vortex formation.

3   Experimental Results and Discussion

3.1   Flow Pattern

Figures 3 through 5, are a sequence of photos taken at a fixed location for a typical flow pattern: a $2.0s$ wave train propagates in the wave tank with still water depth $h = 0.297m$ in the constant depth region. The direction of wave propagation was from left to right in all the photos presented below. They show the vortices migrating in the offshore direction (left) as reflected by the movement of the dye. The pictures were taken 2 m offshore from the injection point five seconds apart. They clearly show that there are two layers of vortices: one layer with small vortices exists near the water surface (approximately 0.05 m below water surface), and the other near the mid-depth (approximately 0.1 m below water surface). Vortices near the water surface rotate in the opposite direction of vortices at mid-depth. For example, for the surface wave propagating to the right, the rotation direction of vortices near mid-depth was observed to be counterclockwise as shown by Matsunaga et al. (1994), while the rotation direction of vortices upper in the water column was observed to be clockwise. The upper layer vortices migrate in the same offshore direction as the lower layer vortices, propagate at the same slow speed as the lower layer vortices, and have the same separation distance as those in the lower layer.
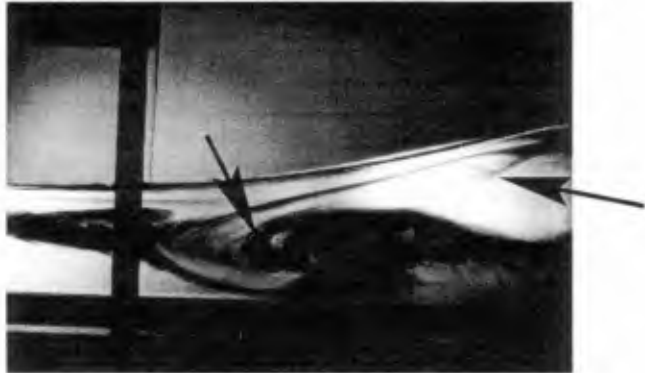

Figure 3: Dye pattern of vortices, 150 wave periods after dye injection. The water wave propagates from left to right.

The velocity of the vortex migrating offshore V_{vm} was obtained by determining the time taken for a vortex to move a given distance. For example, the surface wave phase speed for Test 2 is $C = 1.33m/s$, average instabilities speed is $V_{vm} = 0.0072m/s$. The average rotating time of vortices T_{rot} is 21.5 s, about 10 times of the surface wave period. These vortices in the offshore direction migrate with the speed slower than the undertow. They rotate with longer time than the water particle orbital motions.
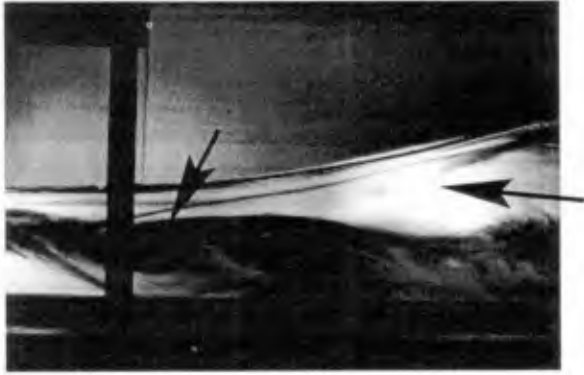
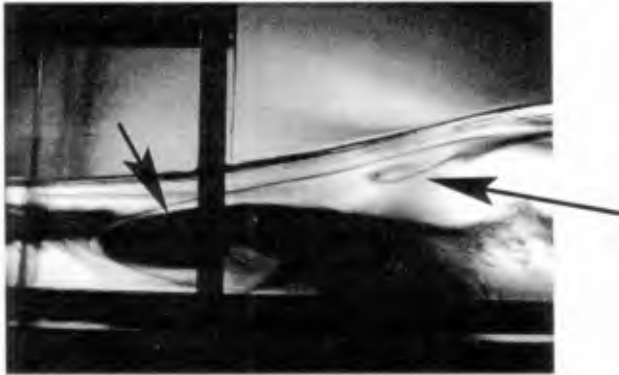Figure 4: Dye pattern of vortices, 155 wave periods after dye injection.

Figure 5: Dye pattern of vortices, 160.9 wave periods after dye injection.

3.2   Mean Velocity Profile

The measured velocity u, w can be split into 4 components: a steady wave-induced current component U, longer time scale components u_{vor}, w_{vor} due to the vortices, the orbital wave motions components u_w, w_w and turbulent components u_t, w_t. The velocity due to the vortices is defined as angular frequencies less than $1.25\ Hz$ for test 1 through 8. The $\overline{u_t w_t}$ represents the turbulent contribution to the momentum transfer, whereas the $\overline{u_w w_w}$ and the $\overline{u_{vor} w_{vor}}$ represent the wave contribution and the vortices contribution, respectively. The average $\overline{u_{vor} w_{vor}}/\overline{u_w w_w}$ is less than 10%, implying that the vortices contribution to the momentum transfer is insignificant compare to the wave contribution.

The mean velocity profiles measured by the ADV for the eight experiments are shown in figure 6. When we filtered the high frequency components, the mean velocity was obtained from low frequency component which includes the mean current and the longer time scale component. From figure 6, the velocity profiles are curved over the depth. Changes in the curvature of these profiles correspond to the presence of shear layers, there are two shear layers existing over the depth. Tests 7 and 8 show linear distribution over the depth.
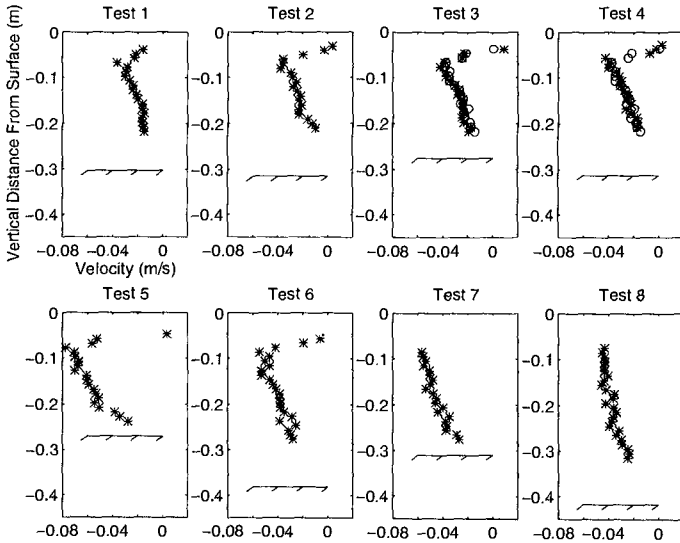

Figure 6: Undertow profile for each test versus depth.

3.3   Long Time Scale Component Velocity Profile

Figure 7 shows the distribution of horizontal velocity of the low frequency component due to vortices for Test 1 and 2. The root-mean-square value $u_{vor_{rms}}$ were obtained by using the low pass filter. The cutoff frequency is $0.2\ Hz$, while the sampling frequency is $50\ Hz$. The velocity profile for longer time component is uniformly distributed. The
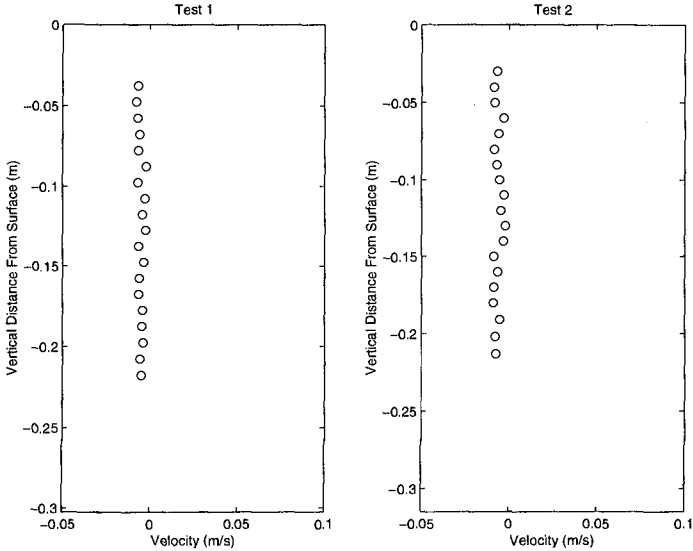

Figure 7: Undertow profile for each test versus depth.

speed of vortices with long time scale is much slower than the undertow. It indicate that upper layer vortices migrate in the same offshore direction as the lower layer vortices and propagate at the same slow speed as the lower layer vortices, which was shown by the dye pattern.

3.4   Nonlinearity

In figure 2, line (c) is the boundary of nonlinearity. Ursell number Ur represents the ratio of wave nonlinearity to frequency dispersion. The importance of nonlinearity of the surface wave to the presence of the vortices is discussed here. The value of Ur for all eight tests are shown in Table 2. For the tests that vortices were observed (tests 1 through 6), Ursell numbers are higher, and lower Ursell numbers exist for the tests that no vortices were noticed (tests 7 through 8). Thus the nonlinearity of the surface wave is important for the presence of vortices.

Table 2: Ursell Number

Test	1	2	3	4	5	6	7	8
Ur	0.4357	0.4000	0.5652	0.4319	0.3844	0.1773	0.1413	0.0664

4　Theoretical Analysis

4.1　Stability Equation

The experimental study shows that the vortices are embedded in orbital wave motion, have longer time scales and shorter length scales than the incident waves. Therefore, the velocity u, w consist of a steady wave-induced current component U, longer time scale components u_{vor}, w_{vor} due to the vortices, the orbital wave motions components u_w, w_w, and turbulent components u_t, w_t.

For the study of fluid motion outside of the surf zone when surface wave runs up at the beach, viscosity should be considered. The governing equations for the homogeneous and incompressible flow is the Navier-Stokes equations and continuity equation. As shown in Li and Dalrymple (1998), the nondimensional equation for the longer time scale motion can be obtained by averaging first over the high frequency turbulence scale, and then over the orbital wave period.

$$\frac{\partial \vec{u_R}}{\partial t} + (\vec{u_R} \cdot \nabla)\vec{u_R} = -\nabla p + \frac{1}{Re} \nabla^2 \vec{u_R} - \vec{R_t} - \vec{R_w} \qquad (1)$$

where $\vec{u_R} = \{U + u_{vor}, w_{vor}\}$. Re is Reynolds number $U_{ref}L_{ref}/\nu \gg 1$. ν denotes the kinematic viscosity. L_{ref} is the water depth. U_{ref} is the maximum velocity of the undertow. The turbulent stresses $R_{t_x} = \frac{\partial \overline{\widetilde{u_t^2}}}{\partial x} + \frac{\partial \overline{\widetilde{u_t w_t}}}{\partial z}$, $R_{t_z} = \frac{\partial \overline{\widetilde{u_t w_t}}}{\partial x} + \frac{\partial \overline{\widetilde{w_t^2}}}{\partial z}$. R_w denotes the time-averaged Reynolds stress resulting from the wave field (Radiation stress): $R_{w_x} = \frac{\partial \overline{u_w^2}}{\partial x} + \frac{\partial \overline{u_w w_w}}{\partial z}$, $R_{w_z} = \frac{\partial \overline{u_w w_w}}{\partial x} + \frac{\partial \overline{w_w^2}}{\partial z}$.

As shown in Li and Dalrymple (1998), through a perturbation analysis of equation 1, at the zeroth order the governing equations for the mean flow are obtained, and at the first order the equations of the interaction between disturbances and mean flow are generated. The equation of the interaction between disturbances and mean flow is the Orr-Sommerfeld equation which governs the stability of fluid motion:

$$\frac{1}{i\alpha Re}(D^2 - \alpha^2)^2 \phi = (U - c)(D^2 - \alpha^2)\phi - U''\phi \qquad (2)$$

where $D\phi = \phi'$. $\psi(x, z, t) = \phi(z)e^{i\alpha(x-ct)}$, ψ is a stream function, α is the wave number and c is the wave phase speed.

The wave number α is real. Solutions of the Orr-Sommerfeld equation are progressive disturbance waves with phase speed equal to the real part of c. If c has a negative imaginary component, the solution has an exponentially growing amplitude

which indicates that mean velocity profile, $U(z)$, is unstable to perturbations of the velocity field with that wavenumber. In cases where more than one such c are present, it is assumed that the one with the largest imaginary component will dominate the instability of that wavenumber. This correspond to the point of maximum αc_{im}, where c_{im} is the imaginary part of c. If c has zero imaginary component, the solution is neutrally stable to disturbance of the velocity field with that wavenumber.

The boundary conditions are that the normal and shear stresses are zero at the free surface, and the rigid boundary condition applies at the bottom.

Equation 2 is difficult to solve analytically for a general velocity distribution $U(z)$. Therefore, a numerical approach was attempted, which was discussed in Li and Dalrymple (1998).

4.2   Vorticity Equation

The vorticity equation derived from the momentum equations 1 is:

$$\frac{\partial \omega}{\partial t} + (\vec{u_R} \cdot \nabla)\omega = \frac{1}{Re} \nabla^2 \omega + \omega \nabla \cdot \vec{u_R} - \nabla \times \vec{R_t} - \nabla \times \vec{R_w} \tag{3}$$

The first term on the right hand side represents the diffusion of vorticity due to the action of viscosity. $\omega \nabla \cdot \vec{u_R}$ provides the mechanism of vortex stretching. The stress terms due to turbulence and radiation stress serve as the source of vorticity. The vortices that we observed are due to instabilities of the undertow.

5   Numerical Results and Discussions

Since we do not have a theoretical profile of mean velocity with shear layers, the measured undertow profiles will be used in our numerical calculations that follow. The smooth velocity profile was obtained by fitting a 5-th order polynomial to the measured wave-averaged data, Li and Dalrymple (1998). Tests 7 and 8 are neutrally stable to any disturbance to the corresponding mean flow.

Numerical approach was used to predict the vortices generation under the flow conditions similar to the cases in the experimental study. The numerical predictions are then compared with the results measured in the experimental study.

5.1   Numerical Predicted Vortices

As stated in Li and Dalrymple (1998), the numerical instability model successfully obtained single layer vortex, by using the assumed velocity profile based on the deformation of dye lines shown in Matsunaga et al. (1988, 1994). Figure 8 shows the numerically predicted flow for one surface wave wavelength using the undertow velocity profile and water depths of Tests 1 and 2. The stream lines are gained by summing the mean flow and the fasted growing unstable wave. Figure 9 show velocity field and the spatial patterns of the streamlines for a quarter surface wave for Test 2. More

figures of predicted instabilities are shown in Li and Dalrymple (1998). These figures show similar results as the observations in the experiments: there are two layers of unstable waves exist over depth. The rotation direction of vortices near surface was the same as the wave-induced water particle trajectories, while the rotation direction of vortices near mid-depth was in opposite direction. The unstable wavelength is much shorter than the surface wave length.
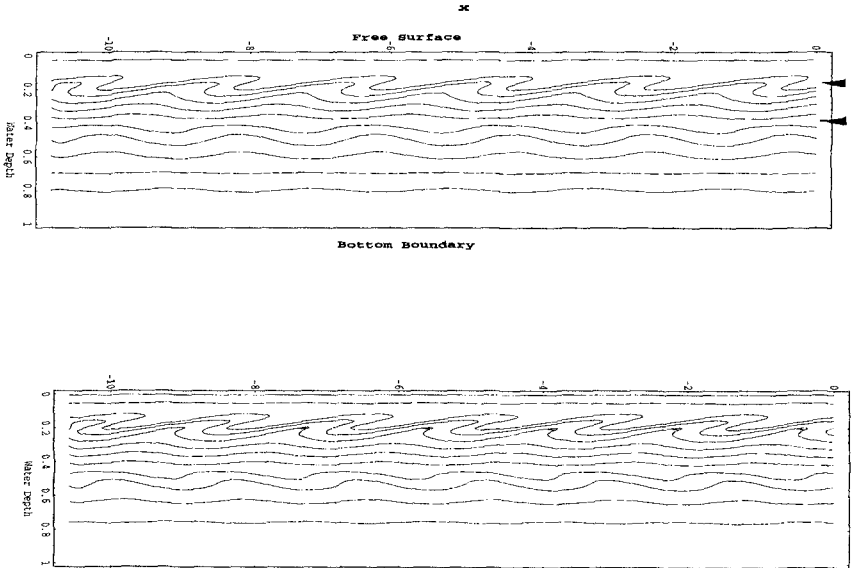

Figure 8: Streamline of the instabilities over one surface wavelength. The surface wave propagates to the left, top: test 1, bottom: test 2.

5.2 Velocity of Vortical Motion

Li and Dalrymple (1998) also showed the good agreement of horizontal length scales and vertical positions between the numerical instabilities and the corresponding experimental results. The experimental and numerical results of the speed of the instabilities are shown in Table 3. Good agreement between the experiment and numerical model is observed. As stated in the experimental study, the instabilities move offshore
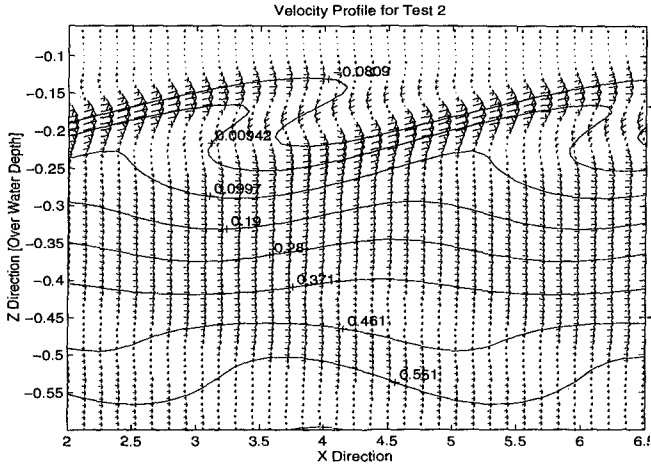
Figure 9: The velocity field for test 2 over a quarter surface wavelength. The surface wave propagates to the left.

Table 3: Comparison between the numerical solution and experimental results

Test	Speed of Vortices in Offshore Direction (m/s)		
	Experiment	Numerical Result	Matsunaga et al. (1994)
1	0.0063	0.0077	0.0112
2	0.0072	0.0070	0.0119
3	0.0069	0.0072	0.0124
4	0.0070	0.0079	0.0133
5	0.0102	0.0140	0.0341
6	0.0056	0.0089	0.0272

slower than the undertow do. Clearly, the linear perturbation model can predict the speed, the position, length scale of the vortices and the existence of the vortex.

6   Conclusions

In this paper, both experimental and numerical studies on the offshore vortex train were conducted. The following conclusions can be drawn.

It has been shown that an undertow seaward of the surf zone can cause oscillations that are different from regular surface waves. These oscillations are below water surface with shorter length scale and longer time scale. Two vortex layers exist over the water depth, because of the existence of two shear layers. The resulting vortices near the water surface rotate in the opposite direction as one at mid-depth. Vortices near the water surface migrate in the same offshore direction as the vortices at mid-depth, propagate at the same speed which is slower than undertow as vortices at mid-depth.

Using the flow conditions similar to those in the experiments, the speed for the instabilities calculated from the numerical model is compared with the corresponding experimental results. Good agreement between the experiment and numerical model is observed. It may be concluded that the linear stability model can predict the occurrence of the vortices from the velocity profile.

The stresses due to turbulence and wave serve as the source of the vorticity. The nonlinearity of the surface wave may play an important role in the presence of vortices.

Reference

Bowen, A.J., 1969 "The Generation of Longshore Currents on a Plane Beach." *J. Marine Res.* , 27, no. 2, 206–215.

Cox, Daniel T., N. Kobayashi & A. Okayasu, 1995 "Vertical Variations of Fluid Velocities and Shear Stress in Surf Zones. " *Proc. 24th Intl. Coastal Engineering Conference*, 1, 98-112.

Craik, A.D.D., 1982 "The Drift Velocity of Water Waves." *J. Fluid Mechanics* , 116, 187–205.

Drazin, P.G. & W.H. Reid, 1981 "Hydrodynamic Stability." Cambridge University Press.

Li, L. & R.A. Dalrymple, 1998 "Instabilities of the Undertow." *J. Fluid Mechanics*, 369, 175-190.

Lin, C.C., 1955 "The Theory of Hydrodynamic Stability." Cambridge University Press.

Longuet-Higgins, M.S., 1953 "Mass Transport in Water Waves." *Phil. Trans. R. Soc. Lond.*, A 245, 535–581.

Matsunaga, N., K. Takehara & Y. Awaya, 1988 " Coherent Eddies Induced by Breakers on a Sloping Bed." *Proc. 21st Intl. Coastal Engineering Conference,* 234–245.

Matsunaga, N., K. Takehara & Y. Awaya, 1994 "The Offshore Vortex Train." *J. Fluid Mechanics,* 276, 113–124.

Nadaoka, K. & T. Kondoh, 1982 "Laboratory Measurements of Velocity Field Structure in the Surf Zone." *Coastal Eng. Jpn.,* 25, 125–145.

Okayasu, A. & H. Katayama, 1992 " Distribution of Undertow and Long-wave Component Velocity Due to Random Waves. " *Proc. 23rd Intl. Coastal Engineering Conference, Venice, Italy, October, 1992,* Chapter 66, 883-893.

Svendsen, I.A. & U. Putrevu, 1992 "A Mixing Mechanism in the Nearshore Region." *Proc. 23rd Intl. Coastal Engineering Conference, Venice, Italy, October, 1992,* Chapter 211, 2758-2771.